Effect of Pt Addition on the Formation of Ni-Pt Porous Layer

著者	Nakajima Kano, Takahashi Hiroki, Fukumoto Michihisa
journal or publication title	COATINGS
volume	12
number	11
year	2022
出版者	MDPI
関連リンク	http://dx.doi.org/10.3390/coatings12111645(http://dx.doi.org/10.3390/coatings12111645)
著作権等	(C) 2022 by the authors. Licensee MDPI, Basel, Switzerland. This article is an open access article distributed under the terms and conditions of the Creative Commons Attribution (CC BY) license (http://creativecommons.org/licenses/by/4.0/).
URL	http://hdl.handle.net/10295/00006253

doi: 10.3390/coatings12111645

coatings

MDPI

Article

Effect of Pt Addition on the Formation of Ni–Pt Porous Layer

Kano Nakajima, Hiroki Takahashi and Michihisa Fukumoto *

Graduate School of Engineering, Akita University, Akita 010-8502, Japan
* Correspondence: fukumoto@gipc.akita-u.ac.jp; Tel.: +81-18-889-2426

Abstract: A Ni–Pt alloy porous layer was formed by electrodepositing Pt using Ni as the substrate sample, followed by Al-depositing and Al-dissolving. The Pt was electrolyzed using an aqueous solution as the medium, and the Al-depositing and Al-dissolving were treated using a molten salt as the medium. The molten salt used was NaCl–KCl with 3.5 mol% AlF_3 added. It was found that Pt electrodeposition formed on the surface had a finer structure. Furthermore, it was clarified that the lower the electrodeposition potential, the thicker the Ni-Pt alloy porous layer. The cathode polarization curve was measured in KOH solution, and the hydrogen gas was determined when a constant voltage electrolysis was performed with a hydrogen detection gas sensor using a tubular yttria-stabilized zirconia (8 mol% Y_2O_3–ZrO_2).

Keywords: hydrogen electrode; Ni–Pt alloy; hydrogen formation; oxygen-pump sensor

1. Introduction

Greenhouse gases are generated by the use of fossil fuels, and global warming has become a major problem. Therefore, greenhouse gas emissions need to be suppressed. Hydrogen energy, that does not emit greenhouse gases, is drawing attention [1,2]. At present, it is required to inexpensively generate hydrogen produced by alkaline water electrolysis. The cathode electrodes have been developed to generate hydrogen with a high efficiency [3–17]. Ni alloys such as Ni–Zr alloys, Ni–Al alloys, Ni–Fe alloys and Ni–Cu alloys are considered useful as electrode materials.Until now, Ni alloys have been mainly used for cathode electrodes because of their good corrosion resistance in alkaline water [8–17]. Pt is a catalytically active metal. The Ni–Pt alloy is considered to be promising for further improving the performance [18–20]. Moreover, to improve the characteristics of this Ni–Pt alloy, it is necessary to make it porous. However, there is a problem that the price is high.

The authors have used molten salts to easily form porous surface layers of various alloys [21,22]. In this study, improving the electrode performance by forming an alloy containing Pt only on the surface by Pt electrodeposition used as a catalyst was investigated. Figure 1 shows the method of forming the Ni–Pt alloy porous surface applied in this study. First, Pt is electrodeposited using an aqueous solution as a medium (a). Next, Al is electrodeposited using the molten salt as a medium (b). At this time, the electrodeposited Al reacts with Pt and the base material Ni to form an alloy in order to carry out the experiment at high temperature (c). The authors have clarified that Ni–Al is formed by Al electrodeposition using Ni as a substrate [23]. A porous layer of Ni–Pt alloy is then formed by dissolving only the Al (d). A porous surface of the Ni–Pt alloy can be formed only on the surface. As a result, the amount of Pt used can be reduced. The hydrogen formation of the generated porous Ni–Pt surface layer in an alkaline aqueous solution will be investigated.

It is difficult to measure the hydrogen by alkaline water electrolysis in situ. The authors have in-situ measured hydrogen generated using ZrO_2–Y_2O_3, which is a solid electrolyte. It was clarified that a small amount of hydrogen can be accurately measured in situ [24,25].

check for updates

Citation: Nakajima, K.; Takahashi, H.; Fukumoto, M. Effect of Pt Addition on the Formation of Ni–Pt Porous Layer. *Coatings* **2022**, *12*, 1645. https://doi.org/10.3390/coatings12111645

Academic Editor: Stefano Caporali

Received: 3 October 2022
Accepted: 28 October 2022
Published: 30 October 2022

Publisher's Note: MDPI stays neutral with regard to jurisdictional claims in published maps and institutional affiliations.

Copyright: © 2022 by the authors. Licensee MDPI, Basel, Switzerland. This article is an open access article distributed under the terms and conditions of the Creative Commons Attribution (CC BY) license (https://creativecommons.org/licenses/by/4.0/).

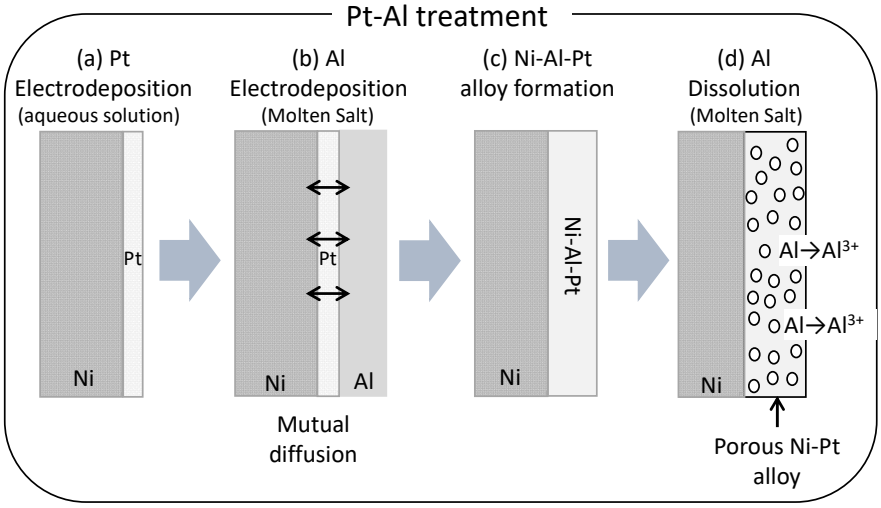

Figure 1. Method of the Ni–Pt alloy porous layer formation.

This study is to prepare a porous Ni–Pt alloy by Pt electrodeposition and porous treatment in a molten salt, and to measure cathodic polarization curve. The Ni–Pt porous layer was observed by SEM (JEOL, Tokyo, Japan), and the phase was identified by an X-ray analysis. The cathode polarization curve in 10 mass% KOH was measured, and the hydrogen was measured in situ using a hydrogen detection sensor, called an oxygen pump-sensor, in order to evaluate the cathode performance. The relationship with the amount of hydrogen generated under the formation conditions of the Ni–Pt alloy porous layer was then clarified.

2. Experimental Procedure

The substrate was Ni, which is used for electrodes in alkaline water electrolysis. The surface of the sample was polished to No. 800 with emery paper, then ultrasonically cleaned in acetone. The surface area of the sample was 2 cm^2. Pt was electrodeposited using a commercial plating solution (NIPPON CHEMICAL INDUSTRIAL Co., Ltd., Tokyo, Japan) under the conditions of a 20 mA cm^{-2} current density at 50 °C and for 30 min. The Counter electrode is Pt mesh (2 cm^2).

The Ni–Pt–Al alloy was then formed and only Al was dissolved to form a porous layer. Therefore, Al was electrodeposited and dissolved. Only Al was then dissolved in the same molten salt to prepare a porous layer after the Al electrodeposition.

The electrolytic cell used in this experiment was described in a previous report [23]. A graphite rod was used as the counter electrode. The bath temperature for the Al electrodeposition and Al dissolution was 750 °C. Ar gas was flowed into the cell during the experiment. Al was electrodeposited at −1.8 V. Al was electrodeposited for 30 min and 60 min only at −1.8 V. At the other potentials, Al was electrolyzed by a constant potential electrolysis for 30 min. The Al was then dissolved at −0.5 V in all the samples. Al was dissolved until the anode current became zero. The cross section of the sample after treatment was observed and analyzed by a scanning electron microscope and an X-ray microanalyzer (JEOL, Tokyo, Japan). Furthermore, the formation layer was identified by the X-ray diffraction method. X-ray source was CuKα rays.

The cathode polarization curve was measured in a 10 mass% KOH solution. The measurement was performed in the cathode direction until the potential became −1.25 V from the natural immersion potential.

Furthermore, the amount of hydrogen generated during the electrolysis was observed in situ using a gas sensor. Figure 2 shows a schematic diagram of the equipment used to measure the hydrogen formed by the electrolysis. In this way, the electrolysis was performed between both electrodes at 3.0 V in a 10 mass% KOH.

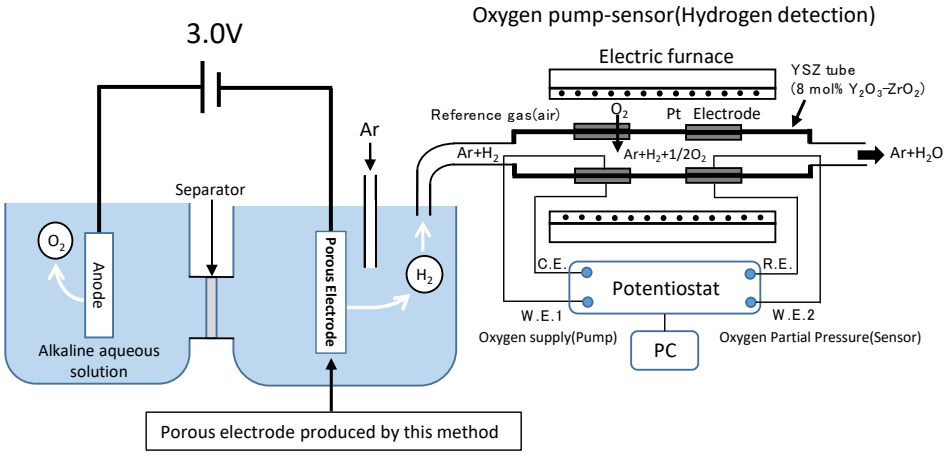

Figure 2. Schematic diagram of hydrogen generation amount measuring device by alkaline water electrolysis.

Figure 3 shows a detailed diagram and principle of the oxygen pump and sensor. As shown in Figure 3a, the tubular yttria-stabilized zirconia (8 mol% Y_2O_3–ZrO_2) was used as the oxygen pump sensor. The measurement gas flows in the YSZ-tube. The oxygen pump sensor consists of a sensor part and a pump part. The Pt was used for the electrodes. The potential was controlled by the sensor part so that the desired oxygen partial pressure was achieved. Details of the hydrogen generation rate are shown in reference [25].

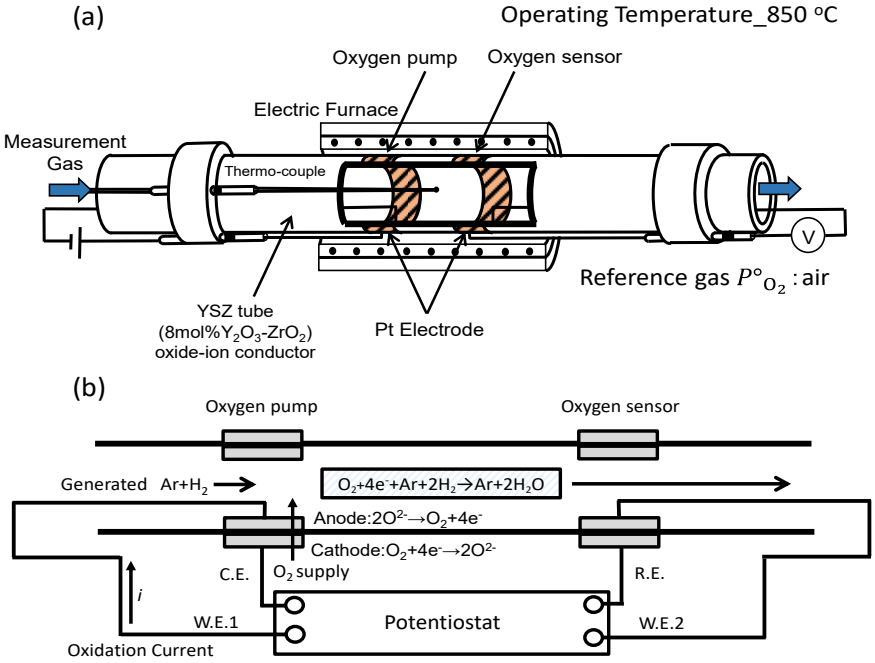

Figure 3. Schematic diagram of oxygen pump sensor for hydrogen content measurement. (**a**) Overall view, (**b**) Principle diagram.

3. Results and Discussion

3.1. Cross-Sectional Microstructure of the Sample Obtained by Electrodepositing Pt

Figure 4 shows the cross-section and the elemental mapping of the Ni and Pt of the sample obtained by electrodeposition Pt at a current density of 20 mA cm^{-2} for 30 min. It was found that an electrodeposition layer of about 5 µm was formed based on the cross-sectional microstructure. The formed electrodeposition layer had a uniform thickness. The adhesion between the electrodeposition layer and the Ni substrate was good, and no

spalling of the Pt electrodeposition layer was observed. An electrodeposition layer of a Pt single layer was formed as a result of the elemental analysis.

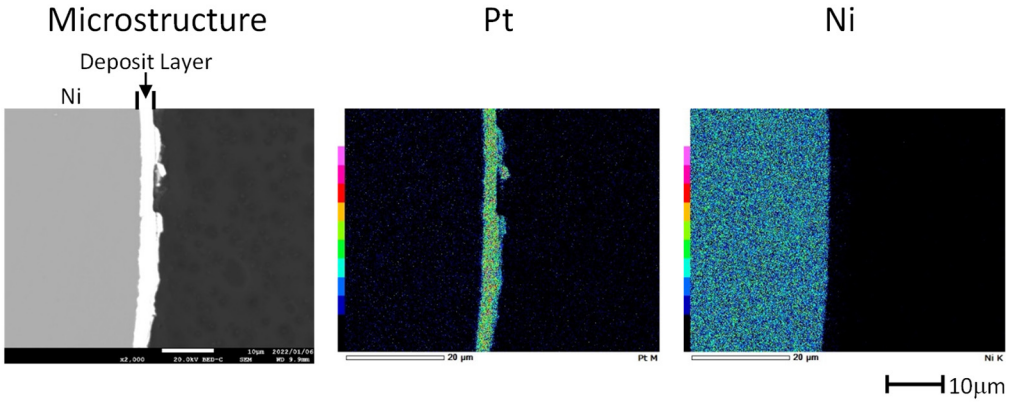

Figure 4. Cross-sectional microstructure and element analysis of Pt-deposited sample on Ni substrate.

3.2. Morphology of Pt–Al-Treated Samples

Figure 5 shows the cross-sectional microstructure and point analysis results of Al electrodeposition-treated sample at −1.8 V after Pt electrodeposition. The Al was 55.7 at.% and Ni was 44.3 at.% at point 1 for Al −1.8 V, 30 min. No Pt content was observed in this layer. The Al was 72.5 at.% and Ni was 24.5 at.%, and $NiAl_3$ was formed at point 2. A small amount of Pt was observed in this $NiAl_3$. An Al monolayer was observed at point 3. The sample with the Al electrodeposition time of 60 min showed the same layer morphology as the sample with the Al electrodeposition of 30 min.

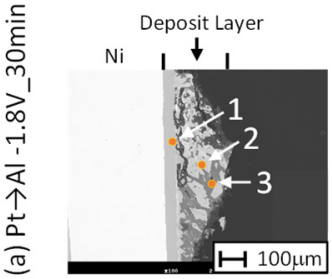

at.%

Point	Ni	Pt	Al
1	44±0.3	0±0.2	55±0.7
2	24±0.5	3±0.1	72±0.5
3	3±0.3	0±0.2	96±0.7

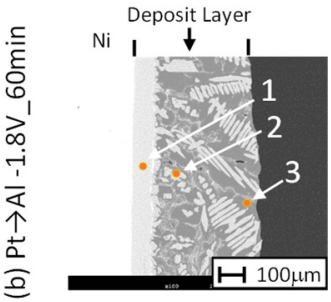

at.%

Point	Ni	Pt	Al
1	42±0.8	0±0.2	57±0.2
2	25±0.1	2±0.2	73±0.2
3	4±0.3	0±0.2	95±0.1

Figure 5. Cross-sectional microstructure and point analysis results of Al electrodeposition-treated sample at −1.8V after Pt electrodeposition.

Figure 6 shows the surface of a treated sample (Pt–Al Treatment) with Al electrodeposition-dissolution after Pt electrodeposition. The experiment was carried out by changing the electrodeposition time of Al after the electrodeposition of Pt. It can be seen that all the samples are not flat. Furthermore, it was in the form of fine particles, and the many cracks were observed. In particular, many fine cracks were observed in the sample.

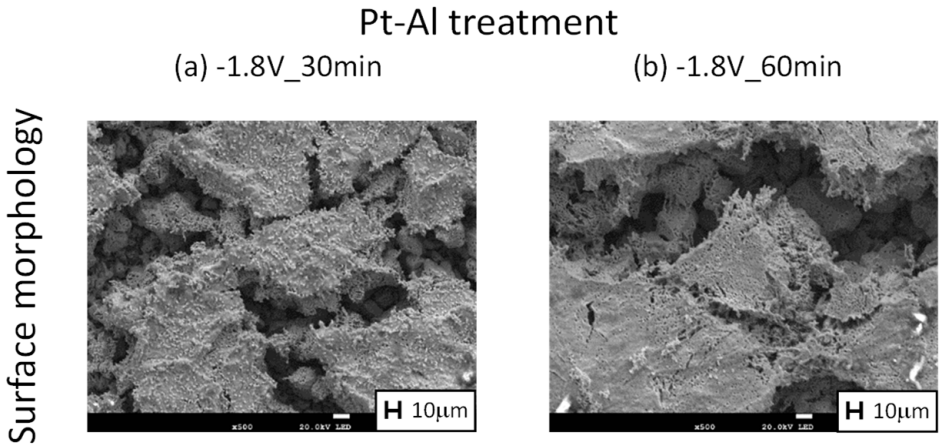

Figure 6. Surface morphology of Al porous sample after Pt electrodeposition. (**a**) Al electrodeposition −1.8 V, 30 min, (**b**) Al electrodeposition −1.8 V, 60 min.

Figure 7 shows the X-ray diffraction patterns for Pt-Al treatment (a) −1.8 V for 30 min and (b) −1.8 V for 60 min. The electrolytic conditions for Al are −1.8 V, 30 min and 60 min. Only the Ni peak was observed regardless of the Al electrodeposition conditions in the Al electrodeposition-dissolved sample after the Pt electrodeposition. This is because in the phase diagram [26], Ni and Pt do not change their crystal structure and Pt replaces the position of Ni. Therefore, only the peak of Ni was observed. It is considered that Pt is dissolved in Ni.

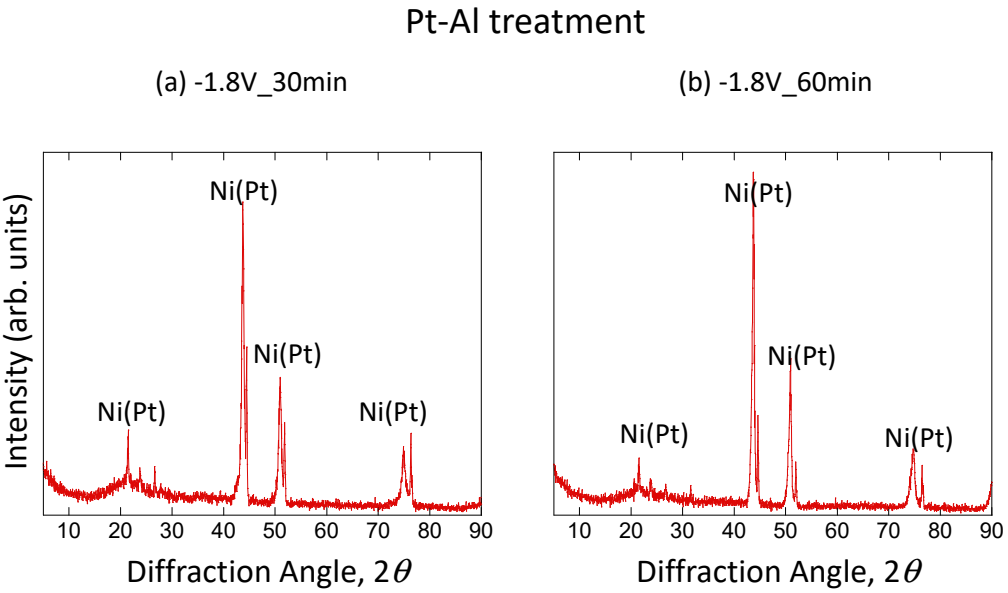

Figure 7. X-ray diffraction patterns for Pt-Al treatment (**a**) −1.8 V for 30 min and (**b**) −1.8 V for 60 min.

Figure 8 shows the cross-sectional microstructure and the results of a point analysis of the porous treated sample of the Al electrodeposition-dissolution after Pt electrodeposition. For (a), the Pt concentration in the outer layer of the Ni–Pt alloy porous layer was 15.0 at.% (Point 1). However, it decreased to 4.3 at.% in the sample of (b) (Point 1). It is considered that this is because Pt diffused due to the longer electrodeposition time. It was clarified that the Pt concentration of the surface Ni–Pt alloy changes by changing the electrodeposition conditions of Al.

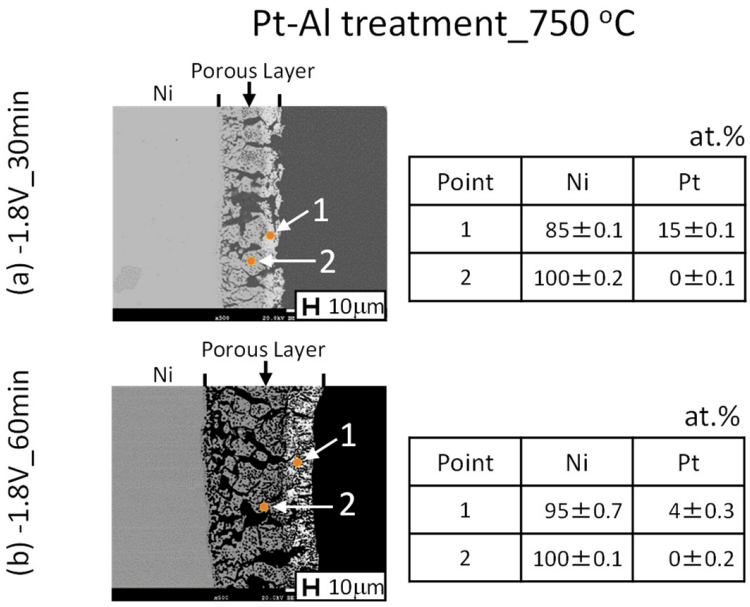

at.%

Point	Ni	Pt
1	85±0.1	15±0.1
2	100±0.2	0±0.1

at.%

Point	Ni	Pt
1	95±0.7	4±0.3
2	100±0.1	0±0.2

Figure 8. Cross-sectional microstructure and point analysis results of the sample Al-deposited and Al-dissolved under (**a**) −1.8 V for 30 min and (**b**) −1.8 V for 60 min each condition after Pt.

3.3. Measurement of Hydrogen of the Formed Porous Ni and Ni-Pt Alloys

Figure 9 shows the cathode polarization curves of the only Al treatment and Pt-Al treatment measured in 10 mass% KOH. It was found that the cathode current density increased due to the porosity treatment. The cathode current of the Al-only treated sample was higher than that of the untreated sample. In addition, the cathode current density of the porous-treated sample after the electrodeposition of Pt is dramatically higher than that of the porous-treated sample without Pt. Cathodic polarization curve results show higher performance than previously reported [18–20]. In other words, it was found that the hydrogen generation performance was improved by forming a Ni–Pt alloy. Surface roughness contributes to this phenomenon.

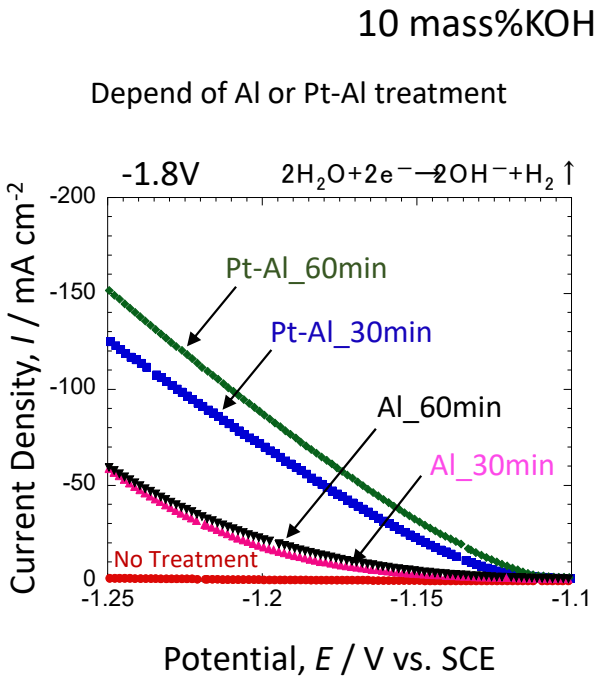

Figure 9. Cathode polarization curve of a sample with a porous surface in a 10 mass% KOH solution.

Figure 10 shows the amount of hydrogen formation at the cathode electrode when electrolyzed at 3.0 V in 10 mass% KOH. For (a), no significant difference from the untreated sample was observed depending on the presence or absence of the Pt electrodeposition when the electrodeposition conditions of Al were −1.8 V and 60 min. However, the amount of generated hydrogen sharply increased when the electrodeposition condition of Al was −1.8 V and 30 min. At this time, hydrogen is rapidly generated during the initial stage of electrolysis. Especially, the amount of generated hydrogen sharply increased after 40 min in the sample in which the Ni-Pt porosity was formed. After the experiment, the electrode was stable without deterioration. For (b), the hydrogen generation behavior of porous Ni–Co, which is the result of past research, is shown [25]. From this, it was clarified that the addition of Pt dramatically increased the amount of hydrogen generation.

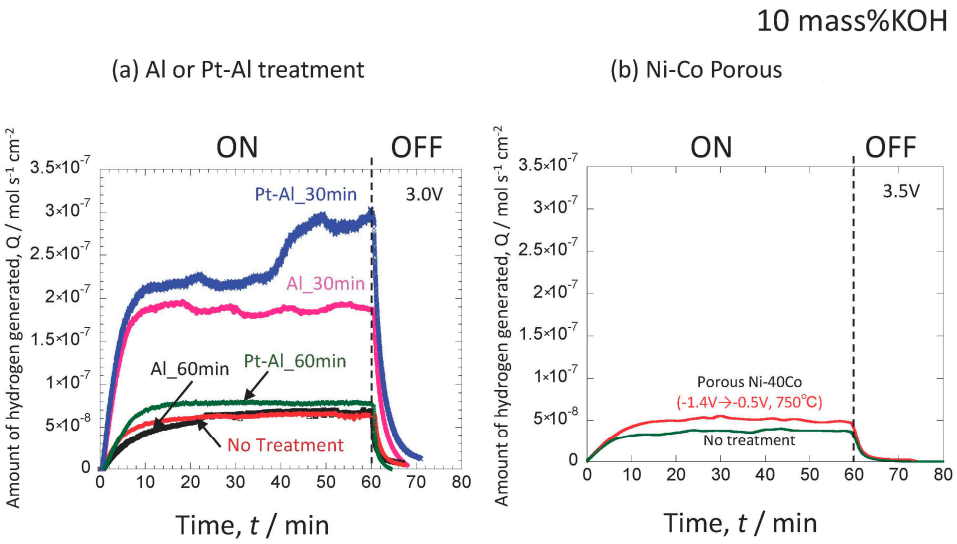

Figure 10. Time dependence of the amount of hydrogen generated measured by the oxygen pump sensor under each condition of (**a**) Al and Pt-Al porosity treatment and (**b**) Ni-Co porosity treatment [25].

Table 1 shows a comparison with past research results. This is the total hydrogen generation rate calculated by integrating Figure 10. Addition of Pt in this way dramatically increases the amount of hydrogen generation.

Table 1. Relationship between each processing condition and the total hydrogen generation amount.

	No Treatment [21]	**Al**	**Pt-Al**	**Previous Study (Ni–Co) [25]**
Hydrogen Generation [mol]	2.1×10^{-4}	6.2×10^{-4}	8.5×10^{-4}	3.0×10^{-4}

Sample Surface area; 2 cm^2.

4. Conclusions

An electrodeposited layer of the Ni–Al–Pt alloy was formed by performing Al electrodeposition in a molten salt using Ni that had Pt deposited on the substrate. Furthermore, the cathode polarization curve of the prepared porous Ni–Pt alloy surface layer was measured. In addition, the amount of hydrogen generated during the constant voltage electrolysis was measured by an oxygen pump sensor, which is a hydrogen detection gas sensor. The obtained results are shown below.

1. A porous Ni-Pt alloy surface could be prepared by Pt electrodeposition and Al electrodeposition-dissolution in a molten salt, and Pt was concentrated on the porous surface.

2. It was found that the Pt-deposited sample formed a denser surface with more voids. It was clarified that the Ni–Pt alloy porous layer was thickened by setting the electrodeposition potential of Al to −1.8 V for 30 min.

3. Porous Ni–Pt alloys showed higher current densities at lower potentials in the cathode polarization curve compared to the untreated Ni and Al electrodeposition-dissolution treatments. The cathode polarization curve in an alkaline solution showed that the Ni–Pt alloy porous surface layer prepared at the Al electrodeposition potential of −1.8 V was a superior cathode material.

4. The sample that formed the Ni-Pt alloy porous layer generated more hydrogen in the hydrogen generation experiment by constant voltage electrolysis. The performance was dramatically improved compared to previous studies.

5. It was clarified that the porous electrode fabricated by this method exhibits excellent performance.

Author Contributions: Conceptualization, M.F.; methodology, K.N.; validation, K.N., H.T. and M.F.; formal analysis, K.N.; investigation, K.N.; resources, M.F.; data curation, K.N.; writing—original draft preparation, K.N.; writing—review and editing, M.F.; visualization, H.T.; supervision, M.F.; project administration, M.F.; funding acquisition, M.F. All authors have read and agreed to the published version of the manuscript.

Funding: This research received no external funding.

Institutional Review Board Statement: Not applicable.

Informed Consent Statement: Not applicable.

Data Availability Statement: Data is contained within the article.

Conflicts of Interest: The authors declare no conflict of interest.

References

1. Momirlan, M.; Veziroglu, T.N. The properties of hydrogen as fuel tomorrow in sustainable energy system for a cleaner planet. *Int. J. Hydrogen Energy* **2005**, *30*, 795–802. [CrossRef]
2. Safizadeh, F.; Ghali, E.; Houlachi, G. Electrocatalysis developments for hydrogen evolutuion reaction in alkaline solutions—A Review. *Int. J. Hydrogen Energy* **2015**, *40*, 256–274. [CrossRef]
3. Chen, L.; Lasia, A. Study of the Kinetics of Hydrogen Evolution Reaction on Nickel-Zinc Alloy Electrodes. *J. Electrochem. Soc.* **1991**, *138*, 3321–3328. [CrossRef]
4. Chen, L.; Lasia, A. Study of the kinetics of hydrogen evolution reaction on nickel-zinc powder electrodes. *J. Electrochem. Soc.* **1992**, *139*, 3214–3219. [CrossRef]
5. Rami, A.; Lasia, A. Kinetics of hydrogen evolution on Ni-Al alloy electrodes. *J. Appl. Electrochem.* **1992**, *22*, 376–382. [CrossRef]
6. Birry, L.; Lasia, A. Studies of the Hydrogen Evolution Reaction on Raney Nickel–Molybdenum Electrodes. *J. Appl. Electrochem.* **2004**, *34*, 735–749. [CrossRef]
7. Navarro-Flores, E.; Chong, Z.; Omanovic, S. Characterization of Ni, NiMo, NiW and NiFe electroactive coatings as electrocatalysts for hydrogen evolution in an acidic medium. *J. Mol. Catal. A Chem.* **2005**, *226*, 179–197. [CrossRef]
8. Mauer, A.E.; Kirk, D.W.; Thorpe, S.J. The role of iron in the prevention of nickel electrode deactivation in alkaline electrolysis. *Electrochim. Acta.* **2007**, *52*, 3505–3509. [CrossRef]
9. Dong, H.; Lei, T.; He, Y.; Xu, N.; Huang, B.; Liu, C.T. Electrochemical performance of porous Ni3Al electrodes for hydrogen evolution reaction. *Int. J. Hydrogen Energy* **2011**, *36*, 12112–12120. [CrossRef]
10. Mullis, A.; Bigg, T.; Adkins, N. A microstructural investigation of gas atomized Raney type Al-27.5 at.% Ni catalyst precursor alloys. *J. Alloys Compd.* **2015**, *648*, 139–148. [CrossRef]
11. Yu, L.; Lei, T.; Nao, B.; Jiang, Y.; He, Y.; Liu, C.T. Characteristics of a sintered porous Ni–Cu alloy cathode for hydrogen production in a potassium hydroxide solution. *Energy* **2016**, *97*, 498–505. [CrossRef]
12. Brown, I.J.; Sotiropoulos, S. Preparation and characterization of microporous Ni coatings as hydrogen evolving cathodes. *J. Appl. Electrochem.* **2000**, *30*, 107–111. [CrossRef]
13. Tanaka, S.; Hirose, N.; Tanaki, T.; Ogata, Y.H. The effect of tin ingredients on electrocatalytic activity of Raney-Ni prepared by mechanical alloying. *Int. J. Hydrogen Energy* **2001**, *26*, 47–53. [CrossRef]
14. Yüce, A.O.; Döner, A.; Kardaş, G. NiMncomposite electrodes as cathode material for hydrogen evolution reaction in alkaline solution. *Int. J. Hydrogen Energy* **2013**, *38*, 4466–4473. [CrossRef]
15. Chade, D.; Berlouis, L.; Infield, D.; Cruden, A.; Nielsen, P.N.; Mathiesen, T. Evaluation of Raney nickel electrodes prepared by atmospheric plasma spraying for alkaline water electrolysers. *Int. J. Hydrogen Energy* **2013**, *38*, 14380–14390. [CrossRef]
16. Lupi, C.; Dell'Era, A.; Pasquali, M. Nickel–cobalt electrodeposited alloys for hydrogen evolution in alkaline media. *Int. J. Hydrogen Energy* **2009**, *34*, 2101–2106. [CrossRef]

17. González-Buch, C.; Herraiz-Cardona, I.; Ortega, E.; García-Antón, J.; Pérez-Herranz, V. Synthesis and characterization of macroporous Ni, Co and Ni-Co electrocatalytic deposits for hydrogen evolution reaction in alkaline media. *Int. J. Hydrogen Energy* **2013**, *38*, 10157–10169. [CrossRef]
18. Domínguez-Crespo, M.A.; Ramírez-Meneses, E.; Torres-Huerta, A.M.; Garibay-Febles, V.; Philippot, K. Kinetics of hydrogen evolution reaction on stabilized Ni, Pt and Ni-Pt nanoparticles obtained by an organometallic approach. *Int. J. Hydrogen Energy* **2012**, *37*, 4798–4811. [CrossRef]
19. Fiameni, S.; Herraiz-Cardona, I.; Musiani, M.; Pérez-Herranz, V.; Vázquez-Gómez, L.; Verlato, E. The HER in alkaline media on Pt-modified three-dimensional Ni cathodes. *Int. J. Hydrogen Energy* **2012**, *37*, 10507–10516. [CrossRef]
20. Eiler, K.; Suriñach, S.; Sort, J.; Pellicer, E. Mesoporous Ni-rich Ni–Pt thin films: Electrodeposition, characterization and performance toward hydrogen evolution reaction in acidic media. *Appl. Catal. B Environ.* **2020**, *265*, 118597. [CrossRef]
21. Fukumoto, M.; Sugiuchi, K.; Nakajima, K. Formation of porous Ni surface by electrodeposition and dissolution in molten salt. *Int. J. Hydrogen Energy* **2020**, *45*, 28252–28259. [CrossRef]
22. Nakajima, K.; Fukumoto, M. Porous Ni-Co surface formation and analysis of hydrogen generation by gas sensor. *Int. J. Hydrogen Energy* **2021**, *46*, 26263–26271. [CrossRef]
23. Fukumoto, M.; Yokobori, A.; Hara, M. Formation of the β-NiAl containing Hf by the Simultaneous Electrodeposition of Al and Hf using a Molten-Salt and the Cyclic Oxidation Behavior. *Oxid. Met.* **2016**, *85*, 17–28. [CrossRef]
24. Fukumoto, M.; Kawamori, Y.; Hara, M. Investigation of cyclic oxidation in Ar-H2O for NiAl containing Hf or Zr by the combination of a hydrogen sensor and an oxygen pump-sensor. *Corros. Sci.* **2019**, *149*, 68–74. [CrossRef]
25. Fukumoto, M.; Nakajima, K.; Kawamori, Y. Investigation of Alumina Formation and Oxidation Rate of Ni-5 wt% Al-X wt% Cr Alloy Using Hydrogen Sensor and Oxygen Pump Sensor. *Oxid. Met.* **2020**, *94*, 191–204. [CrossRef]
26. Nash, P.; Singleton, M.F. Ni-Pt (Nickel-Platinum). In *Phase Diagrams of Binary Nickel Alloys*; ASM International: Materials Park, OH, USA, 1991; pp. 261–264.